Biosensors and Bioelectronics 142 (2019) 111520

Contents lists available at ScienceDirect

Biosensors and Bioelectronics

journal homepage: www.elsevier.com/locate/bios

Ultrasensitive label-free detection of circulating tumor cells using conductivity matching of two-dimensional semiconductor with cancer cell

Yuanyuan Chen[a], Jian Peng[a,b], Youqun Lai[c], Binghui Wu[b], Liping Sun[a,**], Jian Weng[a,*]

[a] Department of Biomaterials, College of Materials, Xiamen University, Xiamen, 361005, China
[b] Collaborative Innovation Center of Chemistry for Energy Materials, State Key Laboratory for Physical Chemistry of Solid Surfaces, and Department of Chemistry, College of Chemistry and Chemical Engineering, Xiamen University, Xiamen, 361005, China
[c] Department of Radiation Oncology, The First Affiliated Hospital of Xiamen University, Xiamen, 361003, China

ARTICLE INFO

Keywords:
2D semiconductor
MoS_2 nanosheets
Biosensors
Circulating cancer cells
Electrochemical impedance

ABSTRACT

The excellent conductivity matching of two-dimensional (2D) semiconductor nanomaterials (e.g. MoS_2) with cancer cell plays an important role in ultrasensitive label-free impedimetric detection of circulating tumor cells (CTC) (< 1 cell/mL). Firstly, 2D semiconductor materials (e.g. 2D MoS_2) exfoliated by folic acid (FA) is used to construct MoS_2/FA-modified gold electrode (AuE/MoS_2/FA). Then, the fabricated electrode is applied for HeLa cell detection in a linear range from 1 to 10^5 cell/mL with a detection limit of 0.43 cell/mL (S/N = 3). The detection mechanism of high sensitivity might be owing to the electric conductivity matching of MoS_2 (0.14 S/m) to cancer cell (0.13–0.23 S/m). A negligible conductivity change induced by cancer cell will produce a large impedance change of semiconductor electrode. Furthermore, HeLa cells dispersed in healthy blood samples are detected by suggested cytosensor in a linear range from 50 to 10^5 cell/mL with a detection limit of 52.24 cell/mL (S/N = 2). Finally, we demonstrate that the cytosensor is capable of differentiating patients of cervical and liver cancers by the real CTC analysis from healthy control.

1. Introduction

Developing feasible methods with sufficient sensitivity and specificity to detect circulating tumor cells (CTC) have a strong impact in clinic by repressing redundant therapies (Ahmed et al., 2017; Lee et al., 2013; Paterlini-Brechot and Benali, 2007; Plaks et al., 2013; Qian et al., 2015). Existing methods for CTC analysis often need laborious experimental steps, stringent laboratory conditions, expensive instruments and so on (Brindle, 2008; Kim et al., 2013; Shen et al., 2017). The label−free detection of CTC by electrochemical method, without any specialized labeling reagent, would greatly simplify the analysis technique and accelerate its implementation for rapid CTC capture and diagnostics (Hwang et al., 2017; Liu et al., 2010; Xu et al., 2016). As one of non-invasive methods for the characterization of cells, electrochemical impedance spectroscopy (EIS) has been used to provide the frequency-dependent electrical properties of cells involved with cellular physiology or morphology (Feng et al., 2011; Gajasinghe et al., 2016; Green et al., 2016; Hu et al., 2013b; Nwankire et al., 2015; Skourou et al., 2004; Wang et al., 2012). The design of electrode with intermediate conductivity and a bionic structure containing biomolecules would play an important role in improving the sensitivity of electrochemical detection (Sun et al., 2014). Therefore, it remains a challenge to design a sensing element with excellent electric conductivity matching to cancer cell for producing ultrasensitive detection of CTC in clinic.

Compared with excellent conductors, such as graphene (10^4 S/m), the advantage of medium electrical conductivity for semiconductor could be helpful in constructing impedimetric approach (Bardhan et al., 2017; Feng et al., 2012; Maltez-da Costa et al., 2012; Yoon et al., 2013; Yoon et al., 2016). Two-dimensional (2D) semiconductor (e.g. MoS_2), with the mobility of at least 200 $cm^2 V^{-1} s^{-1}$ for a 0.15 eV bandgap (Backes et al., 2015; Ghatak et al., 2011; Lopez-Sanchez et al., 2013; Radisavljevic et al., 2011; Tan et al., 2017; Voiry et al., 2015) and its close electron conductivity to cancer cells (0.14 *vs* 0.13–0.23 S/m) (Das et al., 2014; Laufer et al., 2012), together with easily functionalized surface, would completely meet our requirement for electrode design.

Herein, taken 2D MoS_2 as an example, we developed an alternating current (AC) impedimetric approach for label-free and ultrasensitive detection of CTCs based on the conductivity matching of 2D MoS_2 with cancer cell. In our investigations, 2D MoS_2 stabilized with folic acid

* Corresponding author.
** Corresponding author.
E-mail addresses: sunliping@xmu.edu.cn (L. Sun), jweng@xmu.edu.cn (J. Weng).

https://doi.org/10.1016/j.bios.2019.111520
Received 27 May 2019; Received in revised form 2 July 2019; Accepted 15 July 2019
Available online 16 July 2019
0956-5663/

(MoS_2/FA) was used as the signal indicator and assembled on the gold electrode (AuE) surface to produce MoS_2/FA-modified AuE (AuE/MoS_2/FA), yielding an amplified signal to improve detection sensitivity. FA was immobilized on the MoS_2 surface as the outmost layer to selectively recognize folate receptor (FR)-riched HeLa cells. The as-prepared cytosensor presented high sensitivity and selectivity for the detection of FR-riched HeLa cells. Furthermore, MoS_2/FA-anchored electrode was used to detect the real blood samples from patients of liver and cervical cancer with satisfactory results. Such sensing strategies provide a new way for importing 2D MoS_2 techniques into the non-invasion cytosensing systems.

2. Experimental

2.1. Preparation of AuE/MoS_2/FA electrodes

Prior to the modification, the AuE (Φ = 3 mm) was polished with 0.3 and 0.05 μm alumina slurry, rinsed thoroughly with doubly distilled water between each polishing step, then washed successively with 1:1 nitric acid, ethanol, and doubly distilled water in an ultrasonic bath and dried with a high-purity nitrogen steam. 10 μL of MoS_2/FA suspension (100 μg/mL) and 1 μL of 0.5% Nafion mixture were casted on the pretreated AuE and dried under air. To avoid nonspecific adsorption of serum proteins, AuE was immersed in 1% BSA solution for 5 min and then washed by 10 mM PBS (pH = 7.4) to produce AuE/MoS_2/FA electrodes. The modified electrodes were stored in air prior to use.

2.2. Cancer cell detection by impedance measurement

Alternating current impedance measurements were performed on an electrochemical workstation (CHI660C, CH Instrument) using a 3.0 M KCl–Ag/AgCl as the reference electrode, a platinum (Pt) wire as the auxiliary electrode and AuE/MoS_2/FA electrodes as the work electrodes. Electrodes were immersed in 10 mL of fresh solutions of cell suspensions. A mixture of penicillin and streptomycin (1% v/v, Sigma) was added to the cell suspension to prevent microbial contamination. The impedance was then measured with time continuously at 10 Hz. The data were processed by dividing the impedance measured at given time intervals (R_t) by the initial impedance (R_0) of the electrode immediately following immersion into the cell suspensions, and designed as relative impedance ($Z = R_t/R_0$). All electrodes after incubation in cells were washed twice by PBS to remove the natural sedimentation of cells due to gravity. Impedance measurements were also performed on the AUTOLAB PGSTAT302N electrochemical workstation.

2.3. Analysis of clinical samples

Sixteen tubes of fresh whole blood samples anticoagulated with heparin were obtained from the Department of Radiation Oncology of The First Affiliated Hospital of Xiamen University. Blood samples were kept at 4 °C before use. The impedance measurements were performed accroding to the same procedure as pure samples except that AuE/MoS_2/FA electrodes was immersed in PBS solution when fresh whole blood samples were added.

3. Results and discussion

Detection principle shown in Fig. 1 is that cancer cells immobilized on the 2D semiconductor materials essentially hinder unrestricted current flow from the electrode into the bulk electrolyte and thereby increase the overall electrode impedance when HeLa cells attach on the surface of AuE/SC/FA (Fig. 1a). The conductivity of electrode with intermediate conductivity (0.14 S/m) will decrease 50% when a cancer cell (0.13–0.23 S/m) is immobilized on the electrode surface, which is very sensitive to detect cancer cell. On the contrary, this weak change is unobvious for the electrode with too high or low conductivity. For the electrode with too high conductivity (e.g. graphene of 10^4 S/m), the conductivity change of 0.13–0.23 S/m induced by a cancer cell cannot be showed well (about 1000 cells to produce 1% change), thus resulting in the relativily high detection limit. At the same time, the electrode with too low conductivity (e.g. 10^6 Ω), the resistance change of 10 Ω induced by a cancer cells cannot be showed well (about 1000 cells to produce 1% change), also resulting in a relativily high detection limit. The negatively charged SC/FA would decrease the nonspecific binding of normal cells due to electrostatic repulsion between the negatively charged cell membrane and negatively charged electrode surface, which resulted in unchanged impedance (Fig. 1b and c).

3.1. Preparation and characterization of MoS_2/FA

The layered structure of purchased bulk MoS_2 was confirmed by scanning electron microscope (SEM), energy dispersive X−ray (EDX) spectrum and X-ray diffraction (XRD, Fig. S1) pattern. FA containing several amine and amide groups, carboxyl groups and benzene rings shows stronger binding affinity to MoS_2 than two neighboring MoS_2 layers (0.21 eV) (Guan et al., 2015), benefiting the exfoliation process. Furthermore, FA guarantees the FA-modified electrodes to selectively capture FR-rich tumor cells in our system (Low et al., 2008; Malara et al., 2014). Therefore, FA was selected as the functional group. The MoS_2/FA production parameters are optimized to be 30 h, 0.5 mg/mL FA and pH 8 (Figs. S2–4). UV–vis spectra (Fig. S5a) shows that a few absorption peaks at 372, 444, 609 and 672 nm appeared for MoS_2/FA compared to bulk MoS_2. The peaks at 280 and 372 nm are attributed to the π−π transition of FA (Dantola et al., 2010). The XRD pattern of MoS_2/FA (Fig. S5b) shows that a [002] orientation is observed and some characteristic peaks disappear compared to bulk MoS_2, which indicates that bulk MoS_2 had been successfully exfoliated. Transmission electron microscope (TEM) images (Figs. S6a and b) of exfoliated MoS_2 show that the as-obtained MoS_2/FA is extremely thin 2D flake with the size of 100–200 nm. The structure of MoS_2/FA nanosheets was confirmed by selected area electron diffraction (SAED) pattern and HRTEM image (Figs. S6b–c). The SAED pattern with [100] zone axis (Fig. S6b inset) and corresponding HRTEM image (Fig. S6c) reveal the hexagonal lattice structure with the lattice spacing of 0.27 nm and 0.62 nm assigned to the (100) and (002) planes of MoS_2/FA, respectively. Raman spectrum shows that the two characteristic peaks at 380 and 410 cm^{-1} are assigned to E^1_{2g} and A_{1g} modes of the bulk MoS_2. Compared with the bulk MoS_2, MoS_2/FA sample shows an obvious blue shift of E^1_{2g} peak (Fig. S6d) and no obvious shift of A_{1g} peak, indicating that the MoS_2 was successfully exfoliated with a thickness of 4–10 layers (Li et al., 2012a), which was further confirmed by Atomic Force Microscope (AFM, Fig. S6e). The Mo and S elements uniformly distribute in sheets, indicating the MoS_2/FA had been successfully prepared (Fig. S7). The Fourier transform infra−red (FTIR) spectra shows that C=O, C=C and C–N groups could be seen in MoS_2/FA and FA (Fig. S8), but not in bulk MoS_2. Thermal gravimetric analysis (TGA) indicates that MoS_2 was coated by FA molecules with loading as high as 27.9% (Fig. S6f), which could help in constructing highly sensitive biosensors.

3.2. Electrochemical impedance detection of HeLa cells

The AuE/MoS_2/FA was prepared by dropping the MoS_2/FA ink onto gold electrode. Cyclic voltammetry and impedance behavior of various cells on AuE/MoS_2/FA show that it is possible to detect FR-rich HeLa cells by AuE/MoS_2/FA electrode with electrochemical impedance method (Fig. S9 and Table S1). Then, the mean change in impedance at a fixed frequency (10 Hz) was recorded for HeLa cell with different concentrations and plotted against time (Fig. 2a). The relative impedance was produced by dividing the measured impedance at given time by the initial impedance of the AuE/MoS_2/FA electrode. The relative impedance curve indicates an increase against time and could be fitted to a second-order exponential growth (Eq. (1)), and the fittings of

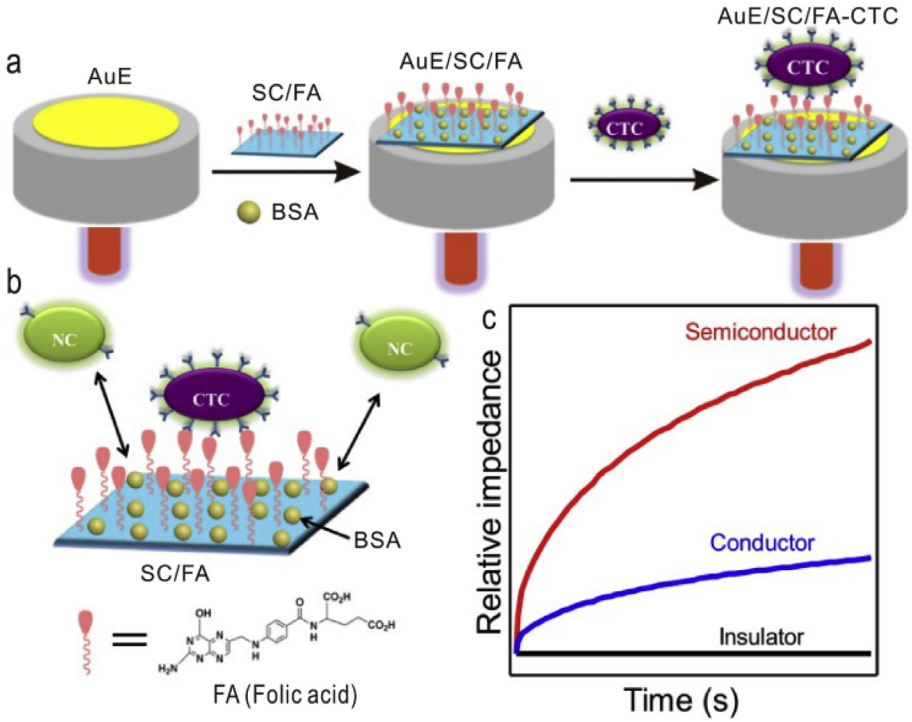

Fig. 1. Schematic diagram of the electrochemical impedance cytosensor with SC/FA probe for detection of CTC. (a) The fabrication of AuE/SC/FA for CTC capture. (b) Schematic model of HeLa cell binding with folic acid (FA) and repelling normal cell (NC) on a negatively charged AuE/ SC/FA electrode surface and (c) the corresponding impedance curves. SC: Semiconductor; AuE: gold electrode; BSA: albumin from bovine serum; CTC: circulating tumor cells; FA: folic acid; NC: normal cells with low folic receptor expression.

exponential association match perfectly with our experimental data (Fig. 2b), resulting from that the detection of HeLa cells on AuE/MoS_2/FA electrode has attachment and immobilization steps and is under mixed mass transport and kinetic control.

$$Z(t) = Z_0 + \Delta Z_1[1 - \exp(-t/\tau_1)] + \Delta Z_2[1 - \exp(-t/\tau_2)] \quad (1)$$

In Eq. (1), Z(t) represents the relative impedance at time of t, Z_0 represents the relative impedance at t = 0, ΔZ_1 and ΔZ_2 represent relative impedances resulted from the cell attachment and binding, τ_1 and

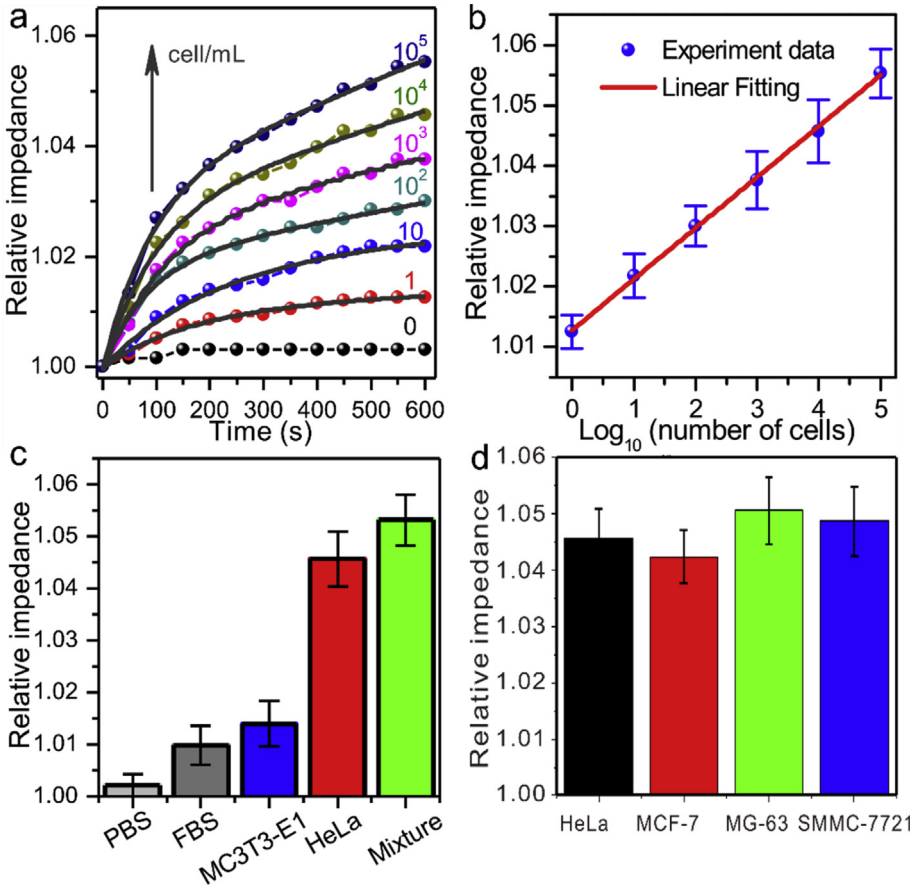

Fig. 2. Ultrasensitive cancer cell detection. (a) Relative impedance at 10 Hz with time for AuE/MoS_2/FA electrodes scanned while being immersed in HeLa cell with different concentrations in PBS. The grey solid lines indicate fittings using exponential association. (b) Calibration plots of relative impedance at 10 min for determining HeLa cells at AuE/MoS_2/FA electrodes while changing the concentration of HeLa cell in PBS. (c) Relative impedance at 10 min at AuE/MoS_2/FA electrodes for PBS, 10% FBS solution, MC3T3-E1 cell suspension, HeLa cell suspension and the mixture of all, indicating a good selectivity of AuE/MoS_2/FA electrodes. (d) Relative impedance at 10 min at AuE/MoS_2/FA electrodes for HeLa, MCF-7, MG-63 and SMMC-7721 cancer cell suspensions. Three replicates were performed.

τ_2 are characteristic attachment and binding times, respectively. The calculated rate constants for cell attachment and binding steps are 0.0065 s^{-1} and 0.02 s^{-1}, respectively. Therefore, the cell attachment is the control step, determining the measurement time. Fitting the all impedance data to Eq. (1) yield the characteristic attachment times τ_{attach} from 468 to 89 s and the binding times τ_{bind} from 133 to 4.3 s with increasing HeLa cell concentration from 1 to 10^5 cell/mL, reaching a final plateau approximately 10 min, which was adopted in the following measurements.

Generally, increasing the concentration of HeLa cells led to faster cell attachment and higher relative impedance, indicating that a higher amount of HeLa cells were immobilized to the surface of the modified electrode. It is not surprizing that the mean impedance against time was dependent on the concentration of HeLa cells. The electrochemical signal was directly related to the amount of cells attached on the surface of the modified electrode. Amaingly, 1 cell/mL of concentration HeLa cell could even be detected using our method (Fig. 2a). The increase of relative impedance against time or cell numbers attached on the surface of electrode is not a simple linear. The concentration of cells in this research was increased from 10° to 10^5 by exponential increasing. Therefore, the increase of relative impedance against the logarithm of the cell number was linear. Fig. 2b shows the calibration plot of relative impedance and logarithmic concentration, linear ($Z = 1.0128 + 0.0084\ Log_{10}\ C$, correlation coefficient of 0.9988) in the concentration of HeLa cells from 1 to 10^5 cell/mL. The detection limit for cell concentration was 0.43 cell/mL (signal to noise ratio is 3), the detection limit of which was much lower than other reports (Table 1).

To explore the selectivity and anti-interference of AuE/MoS_2/FA, relative impedance values of AuE/MoS_2/FA electrodes for PBS, 10% fetal bovine serum (FBS) solution, MC3T3-E1 cell (FA-lack cell line) suspension, HeLa cell suspension and the mixture of all were plotted (Fig. 2c). Compared to buffer medium without any cells and MC3T3-E1 cell, relative impedance value of HeLa cell was much higher, which almost approached relative impedance value of the mixture of all cell suspensions, confirming its specificity to cancer cells (Fig. 2c and Fig. S10). To further confirm the specificity of AuE/MoS_2/FA to cancer cells, the recognition event of few-layer MoS_2 without FA was also investigated (Fig. S11). The ΔR value (1185 ± 35 Ω) and relative impedance of AuE/MoS_2/FA for HeLa cell capturing was much higher than that of AuE/MoS_2/PVA without FA (195 ± 15 Ω), further confirming the specificity of AuE/MoS_2/FA to cancer cells. The similar result is also obtained in glassy carbon electrode (GCE/MoS_2/FA) shown in Fig. S12. The ΔR value (1185 Ω ± 35 Ω) and relative impedance of AuE/MoS_2/FA for HeLa cell capturing were higher than that of GCE/MoS_2/FA (895 Ω ± 25 Ω). So AuE was used in the following investigations.

In order to confirm that the universality of the proposed methodology in electrochemical impedance detection of cells, the representative FR-riched cancer cell lines including MCF-7, MG-63 and SMMC-7721 cell lines were investigated. In Fig. 2d, it can be seen that the impedance responses at AuE/MoS_2/FA electrodes were clearly observed for all test cancer cell lines. This is mainly attributed to the universal immobilization capacity of MoS_2/FA interface for adhesion of FR-rich cells. The difference of the impedance response at AuE/MoS_2/FA electrodes for different cell lines might be attributed to the different amount of FR in different cancer cells.

3.3. Phase contrast microscopy characterization

To further confirm the fact that impedance increasing was really resulted from HeLa cell capture and immobilization, the capture of HeLa cells on the FA-modified electrode surface was further confirmed by transmission-reflecting polarizing microscope (ECLIPSE/Ci-S, Nikon) and phase contrast microscopy (Figs. S13a and b). In order to further observe the cell capture on the electrode surface by phase contrast microscopy, the optically transparent round coverslips (RCS, φ14 mm) were used to replace the gold electrode because it is not optically transparent. As indicated in Figs. S13b–h, with increasing concentration of HeLa cell from 10 to 10^5 cell/mL, HeLa cells immobilized on the MoS_2/FA-coated slides increased, indicating that the biosensing system had a good sensitivity, in good accordance with the result of the EIS method. A large number of cells could be observed on the surface of electrode when the MoS_2/FA-coated slides were incubated with HeLa cells (Fig. 3a). However, there were very few HeLa cells on the surface of electrode when the FA-free MoS_2/PVA-coated slides were incubated with HeLa cells (Fig. 3b). These results indicate that HeLa cells were effectively captured by FA molecules immobilized on the RSC surface. The MoS_2/FA-coated slides was also incubated with FR-lack MC3T3-E1 cells, but only a few cells were adsorbed on the surface of electrode (Fig. 3c), and almost no MC3T3-E1 cell was observed on the surface of blank FA-free MoS_2/PVA-coated slides (Fig. 3d), suggesting the excellent selectivity of the MoS_2/FA-coated slides toward FR-rich cancer cells. The selective detection of HeLa cell in the mixutre of HeLa and MC3T3-E1 cells suspension on MoS_2/FA-coated slides was further confirmed by fluorescence images (Figs. S14 and 15).

3.4. Detection mechanism

To further understand why our sensor is of high sensitivity, the 2D materials with different electric conductivities were also investigated under the similar conditions. For example, 2D MoS_2 was displaced by

Table 1
Sensitivity of various nanomaterials-based cancer cell electrochemical biosensors.

Sensing element	Cancer cell	Transducer	Linear range (cell/mL)	LOD (cell/mL)	Ref.
graphene	HeLa	EIS	10^3–10^6	794	Feng et al. (2011)
ECR	HeLa	DPV	10–10^6	10	Li et al. (2012b)
AuNP/FA	HeLa	EIS	6–10^3 and 10^3–10^5	6	Wang et al. (2012)
Ag@BSA composite	KB	EIS	6–10^8	20	Hu et al. (2013a)
Au/MPA/(Fc-PEI/ SWNT)$_5$/FA	HeLa	DPV	10–10^6	10	Liu et al. (2013)
AuNPs/FA/ferrocene	HeLa	DPV	10–10^6	10	Xu et al. (2013)
GO/PLL	K562	EIS	100–10^7	30	Zhang et al. (2013)
AuNPs-GA-CS	HL-60	ECL	0–5.6 × 10^6	56	Feng et al. (2014)
Fe_3O_4@Au-aptamer	HeLa	ASV	160–15360	89	Jie et al. (2014)
Microfluidic paper	HL-60	DPV	500–7.5 × 10^7	350	Su et al. (2014)
TA/Au/ITO	HeLa	DPV	300–10^7	300	Wang et al. (2014)
BSA/Ag nanoflower	DLD-1	EIS	135–1.35 × 10^7	40	Cao et al. (2015)
supersandwich G-quadruplex DNAzyme	K562	DPV	14–14 × 10^6	14	Lu et al. (2015)
n-SiNPs/PPy	SK-MEL-2	CV	25–3000	8	Seenivasan et al. (2015)
G-quadruplex/hemin/aptamer–AuNPs –HRP	HepG2	DPV	10^2–10^7	6	Sun et al. (2015)
BDD/Au/MUA/FA	HeLa	EIS	10–10^5	10	Previous work (Weng et al., 2011)
MoS_2/FA	HeLa	EIS	1–10^5	0.43	This work

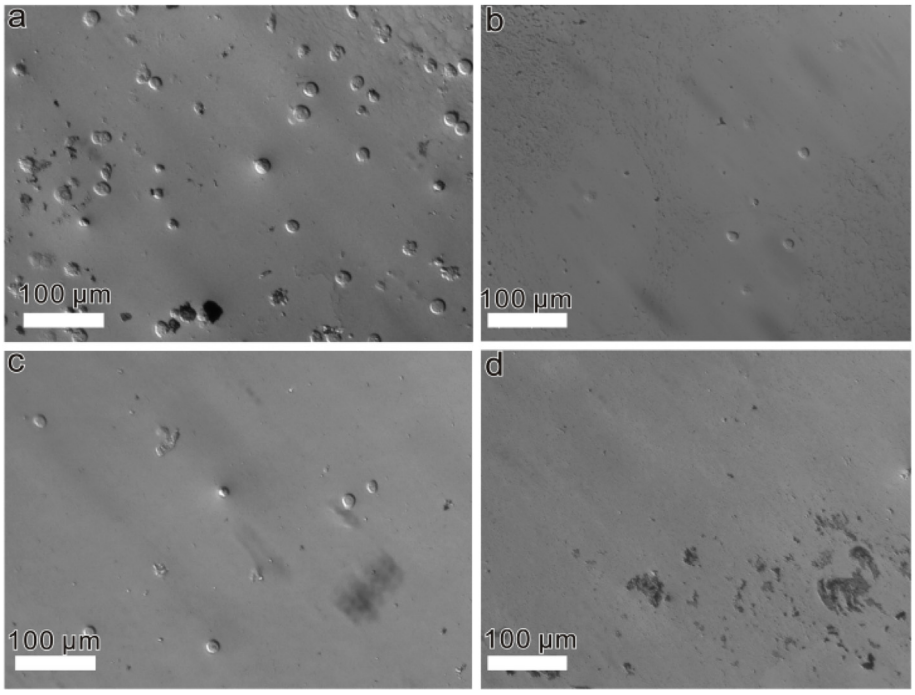

Fig. 3. Microscopy characterization of cancer cells. (a) MoS_2/FA-coated slide incubated with HeLa cells. (b) MoS_2/PVA-coated slide incubated with HeLa cells. (c) MoS_2/FA-coated slide incubated with MT3T3-E1 cells. (d) MoS_2/PVA-coated slides incubated with MT3T3-E1 cells. The concentrations of HeLa and MT3T3-E1 cell suspension are both 10^4 cell/mL, the adsorption time is 30 min.

2D WS_2, Bi_2Se_3, boron nitride (BN) and graphene to prepare WS_2/FA, Bi_2Se_3/FA, BN/FA and graphene/FA electrodes, respectively. The WS_2/FA, Bi_2Se_3/FA, graphene/FA and BN/FA were characterized well by UV–vis spectra, XRD, Raman and AFM technologies (Figs. S16–19). Fig. S20a shows that the relative impedance changes on other four electrodes are smaller than that of AuE/MoS_2/FA and the relative impedance decreased in the following order (MoS_2/FA > WS_2/FA > Bi_2Se_3/FA > graphene/FA > BN/FA, Fig. S20b). Interestingly, the conductivity of these 2D materials increases in the following order: BN < MoS_2 < WS_2 < Bi_2Se_3 < graphene (Table S2). The conductivity of cancer cell (0.13–0.23 S/m) is close to the conductivity of MoS_2 (0.14 S/m), which further confirms our hypothesis that the excellent conductivity matching of 2D semiconductor nanomaterials with cancer cell would play an important role in ultrasensitive detection of cancer cell. Therefore, ultrasensitive detection of tumor cells could be owing to the following three aspects: firstly, 2D MoS_2 with close electron conductivity to that of cancer cells might amplify the impedance change after a few cancer cells were anchored. Secondly, the high FA loading of MoS_2/FA might make sure that even just a few cancer cell could be captured efficiently by our MoS_2/FA, resulting the impedance increasing obviously. Thirdly, the 2D nanosheet structure of MoS_2/FA with high specific surface area might boost the contact sites between 2D semiconductors and cancer cells, thus enhancing the detection sensitivity. At the same time, the high sensivity of this sensor could also be attributed to the field effect and surface charge density change induced by high negative charges in cell membrane of cancer cells (Li et al., 2014; Siek et al., 2018; Weng et al., 2008).

3.5. Application for clinical sample analysis

To explore the feasibility of the developed strategy in biological media, the as-prepared cytosensor was used to detect HeLa cells in human serum. Learned from curve (b) in Fig. 4, the relative resistance at 10 min linearly increased with logarithm of cancer cell concentration from 50 to 10^5 cells/mL by fitting ($\Delta Z = 0.0264\ Log_{10}C$, correlation coefficient of 0.98), with a detection limit of 52.24 cell/mL (S/N = 2), demonstrating the feasibility of the developed strategy for the analysis of real clinical sample. In general, most of the impedance biosensors developed and tested are suffered from complex matrix presented in clinical samples, thus limiting the successful implication of the impedance biosensors for clinical application. To ultimately verify the performance of the proposed biosensor, sixteen clinically acquired samples (four liver cancers, four cervical cancers and 8 healthy people) from the First Hospital of Xiamen University were tested. The detailed experiments were listed in the experimental section and the results were shown in Fig. 4c and d. The relative impedance experienced a large jump when whole blood of cancer patient was added, which was higher than that of healthy people and PBS (Fig. 4c) and the relative impedances measured from cancer patients were significantly higher than those of normal controls (Fig. 4d), indicating that the biosensing could distinguish cancer patients from normal individuals. CTCs were identified in all cervical and liver cancer patients, ranging from 5 to 100 CTCs/mL by flow cytometry offered by the hospital. Interstingly, by using our EIS stratagy, 37.3 ± 2.4 cervical CTCs/mL, 47.2 ± 1.8 liver CTCs/mL but almost no CTCs (mean = 1 ± 0.2 CTCs/mL) in hyperplastic prostate donors and healthy controls were obtained, respectively. This result strongly support that the present approach might be suitable for detection of FR-rich CTC in cancer patients.

4. Conclusion

In summary, we have demonstrated an MoS_2/FA-based label-free electrochemical impedance stratagy for cancer cells detection with a linear detection range from 1 to 10^5 cell/mL and a detection limit of 0.43 cell/mL (S/N = 3). The optimized electrode shows good selectively, universality, and anti-interference for FR-rich cancer cells. The high sensitivity might be attributed to electric conductivity matching of 2D MoS_2 semiconductor to cancer cells. Furthermore, the biosensor could effectively differentiate tumor samples from normal controls. Though the molecular understanding of detection mechanism and practical clinical application is limited, which will be discussed in our future work and extending the concept of 2D semiconductor conductivity matching for DNA and other cancer biomarkers detection as well.

Declaration of competing interest

The authors declare that they have no known competing financial

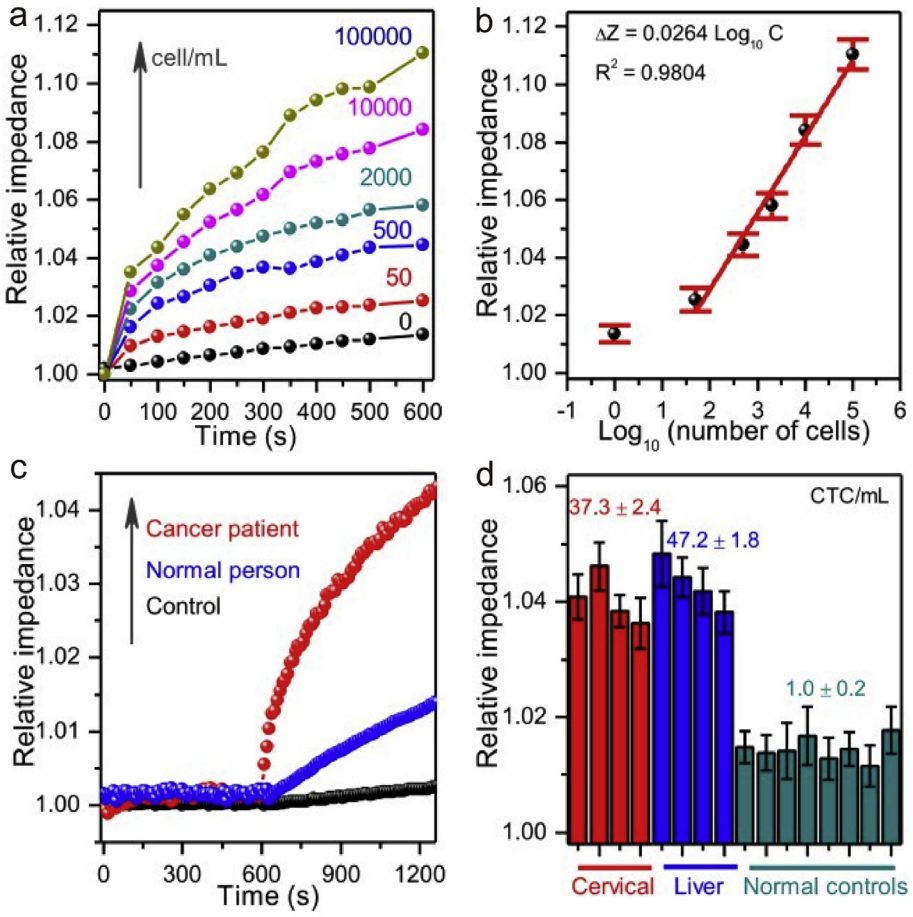

Fig. 4. Application of CTC detection. (a) Relative impedance with time for AuE/MoS_2/FA electrodes scanned while immersed in healthy blood serum samples containing HeLa cells with different concentrations. (b) Calibration plot of relative impedance at 10 min for determining HeLa cells at AuE/MoS_2/FA electrodes while changing the concentration of HeLa cell. (c) Relative impedance with time for AuE/MoS_2/FA electrodes scanned while immersed in PBS for 10 min followed by adding whole blood of cervical cancer patient, healthy people and PBS as control. (d) Relative impedance measured from 16 clinical samples. Cervical and liver represent clinical samples of cervical and liver caners, respectively. Normal controls indicate the samples of healthy people.

interests or personal relationships that could have appeared to influence the work reported in this paper.

The authors declare the following financial interests/personal relationships which may be considered as potential competing interests:

CRediT authorship contribution statement

Yuanyuan Chen: Writing - review & editing, Writing - original draft. **Jian Peng:** Writing - review & editing, Writing - original draft. **Youqun Lai:** Formal analysis, Writing - review & editing, Writing - original draft. **Binghui Wu:** Formal analysis, Writing - review & editing, Writing - original draft. **Liping Sun:** Writing - review & editing, Writing - original draft. **Jian Weng:** Conceptualization, Writing - review & editing, Writing - original draft.

Acknowledgements

Yuanyuan Chen and Jian Peng contributed equally to this work. This work was supported by the National Key Scientific Research Projects (2014CB932004), National Natural Science Foundation of China (81571764, 81872415 and 31371005), China Postdoctoral Science Foundation (2017M612131), the Fundamental Research Funds for the Central Universities and the National Science Foundation of Fujian Province of China (2014H2006).

Appendix A. Supplementary data

Supplementary data to this article can be found online at https://doi.org/10.1016/j.bios.2019.111520.

References

Ahmed, M.G., Abate, M.F., Song, Y., Zhu, Z., Yan, F., Xu, Y., Wang, X., Li, Q., Yang, C., 2017. Angew. Chem. Int. Ed. 56 (36), 10681–10685.
Backes, C., Berner, N.C., Chen, X., Lafargue, P., LaPlace, P., Freeley, M., Duesberg, G.S., Coleman, J.N., McDonald, A.R., 2015. Angew. Chem. Int. Ed. 54 (9), 2638–2642.
Bardhan, N.M., Kumar, P.V., Li, Z., Ploegh, H.L., Grossman, J.C., Belcher, A.M., Chen, G.Y., 2017. ACS Nano 11 (2), 1548–1558.
Brindle, K., 2008. Nat. Rev. Cancer 8 (2), 94–107.
Cao, H.M., Yang, D.P., Ye, D.X., Zhang, X.X., Fang, X.E., Zhang, S., Liu, B.H., Kong, J.L., 2015. Biosens. Bioelectron. 68, 329–335.
Dantola, M.L., Denofrio, M.P., Zurbano, B., Gimenez, C.S., Ogilby, P.R., Lorente, C., Thomas, A.H., 2010. Photochem. Photobiol. Sci. 9 (12), 1604–1612.
Das, D., Kamil, F.A., Biswas, K., Das, S., 2014. RSC Adv. 4 (35), 18178–18185.
Feng, L., Chen, Y., Ren, J., Qu, X., 2011. Biomaterials 32 (11), 2930–2937.
Feng, L., Wu, L., Wang, J., Ren, J., Miyoshi, D., Sugimoto, N., Qu, X., 2012. Adv. Mater. 24 (1), 125–131.
Feng, Q.M., Liu, Z., Chen, H.Y., Xu, J.J., 2014. Electrochem. Commun. 49, 88–92.
Gajasinghe, R.W.R.L., Tigli, O., Jones, M., Ince, T., 2016. IEEE Sens. J. 1–3.
Ghatak, S., Pal, A.N., Ghosh, A., 2011. ACS Nano 5 (10), 7707–7712.
Green, B.J., Saberi Safaei, T., Mepham, A., Labib, M., Mohamadi, R.M., Kelley, S.O., 2016. Angew. Chem. Int. Ed. 55 (4), 1252–1265.
Guan, G., Zhang, S., Liu, S., Cai, Y., Low, M., Teng, C.P., Phang, I.Y., Cheng, Y., Duei, K.L., Srinivasan, B.M., Zheng, Y., Zhang, Y.W., Han, M.Y., 2015. J. Am. Chem. Soc. 137 (19), 6152–6155.
Hu, C.Y., Yang, D.P., Wang, Z.H., Huang, P., Wang, X.S., Chen, D., Cui, D.X., Yang, M., Jia, N.Q., 2013a. Biosens. Bioelectron. 41, 656–662.
Hu, Y., Zuo, P., Ye, B.C., 2013b. Biosens. Bioelectron. 43, 79–83.
Hwang, H.J., Ryu, M.Y., Park, C.Y., Ahn, J., Park, H.G., Choi, C., Ha, S.D., Park, T.J., Park, J.P., 2017. Biosens. Bioelectron. 87, 164–170.
Jie, G.F., Zhang, J., Jie, G.X., Wang, L., 2014. Biosens. Bioelectron. 52, 69–75.
Kim, M.S., Kim, J., Lee, W., Cho, S.J., Oh, J.M., Lee, J.Y., Baek, S., Kim, Y.J., Sim, T.S., Lee, H.J., Jung, G.E., Kim, S.I., Park, J.M., Oh, J.H., Gurel, O., Lee, S.S., Lee, J.G., 2013. Small 9 (18), 3103–3110.
Laufer, S., Solomon, S.B., Rubinsky, B., 2012. Physiol. Meas. 33 (6), 997–1013.
Lee, H.J., Oh, J.H., Oh, J.M., Park, J.M., Lee, J.G., Kim, M.S., Kim, Y.J., Kang, H.J., Jeong, J., Kim, S.I., Lee, S.S., Choi, J.W., Huh, N., 2013. Angew. Chem. Int. Ed. 52 (32), 8337–8340.
Li, B.R., Chen, C.C., Kumar, U.R., Chen, Y.T., 2014. Analyst 139 (7), 1589–1608.
Li, H., Zhang, Q., Yap, C.C.R., Tay, B.K., Edwin, T.H.T., Olivier, A., Baillargeat, D., 2012a.

Adv. Funct. Mater. 22 (7), 1385–1390.
Li, H.L., Li, D., Liu, J.Y., Qin, Y.N., Ren, J.T., Xu, S.L., Liu, Y.Q., Mayer, D., Wang, E.K., 2012b. Chem. Commun. 48 (20), 2594–2596.
Liu, H., Malhotra, R., Peczuh, M.W., Rusling, J.F., 2010. Anal. Chem. 82 (13), 5865–5871.
Liu, J., Qin, Y., Li, D., Wang, T., Liu, Y., Wang, J., Wang, E., 2013. Biosens. Bioelectron. 41, 436–441.
Lopez-Sanchez, O., Lembke, D., Kayci, M., Radenovic, A., Kis, A., 2013. Nat. Nanotechnol. 8 (7), 497–501.
Low, P.S., Henne, W.A., Doorneweerd, D.D., 2008. Acc. Chem. Res. 41 (1), 120–129.
Lu, C.Y., Xu, J.J., Wang, Z.H., Chen, H.Y., 2015. Electrochem. Commun. 52, 49–52.
Malara, N., Coluccio, M.L., Limongi, T., Asande, M., Trunzo, V., Cojoc, G., Raso, C., Candeloro, P., Perozziello, G., Raimondo, R., De Vitis, S., Roveda, L., Renne, M., Prati, U., Mollace, V., Di Fabrizio, E., 2014. Small 10 (21), 4324–4331.
Maltez-da Costa, M., de la Escosura-Muniz, A., Nogues, C., Barrios, L., Ibanez, E., Merkoci, A., 2012. Small 8 (23), 3605–3612.
Nwankire, C.E., Venkatanarayanan, A., Glennon, T., Keyes, T.E., Forster, R.J., Ducree, J., 2015. Biosens. Bioelectron. 68, 382–389.
Paterlini-Brechot, P., Benali, N.L., 2007. Cancer Lett. 253 (2), 180–204.
Plaks, V., Koopman, C.D., Werb, Z., 2013. Science 341 (6151), 1186–1188.
Qian, W.Y., Zhang, Y., Chen, W.Q., 2015. Small 11 (32), 3850–3872.
Radisavljevic, B., Radenovic, A., Brivio, J., Giacometti, V., Kis, A., 2011. Nat. Nanotechnol. 6 (3), 147–150.
Seenivasan, R., Maddodi, N., Setaluri, V., Gunasekaran, S., 2015. Biosens. Bioelectron. 68, 508–515.
Shen, Z., Wu, A., Chen, X., 2017. Current detection technologies for circulating tumor cells. Chem. Soc. Rev. 46 (8), 2038–2056.
Siek, M., Adamkiewicz, W., Sobolev, Y.I., Grzybowski, B.A., 2018. Angew. Chem. Int. Ed. 57 (47), 15379–15383.
Skourou, C., Hoopes, P.J., Strawbridge, R.R., Paulsen, K.D., 2004. Physiol. Meas. 25 (1), 335–346.
Su, M., Ge, L., Ge, S.G., Li, N.Q., Yu, J.H., Yan, M., Huang, J.D., 2014. Anal. Chim. Acta 847, 1–9.
Sun, D.P., Lu, J., Chen, Z.G., Yu, Y.Y., Mo, M.N., 2015. Anal. Chim. Acta 885, 166–173.
Sun, L.P., Hu, N., Peng, J., Chen, L.Y., Weng, J., 2014. Adv. Funct. Mater. 24 (44), 6905–6913.
Tan, C., Cao, X., Wu, X.J., He, Q., Yang, J., Zhang, X., Chen, J., Zhao, W., Han, S., Nam, G.H., Sindoro, M., Zhang, H., 2017. Chem. Rev. 117 (9), 6225–6331.
Voiry, D., Goswami, A., Kappera, R., e Silva Cde, C., Kaplan, D., Fujita, T., Chen, M., Asefa, T., Chhowalla, M., 2015. Nat. Chem. 7 (1), 45–49.
Wang, R.M., Di, J., Ma, J., Ma, Z.F., 2012. Electrochim. Acta 61, 179–184.
Wang, X.B., Ju, J., Li, J., Li, J.Y., Qian, Q.H., Mao, C., Shen, J., 2014. Electrochim. Acta 123, 511–517.
Weng, J., Zhang, J., Li, H., Sun, L., Lin, C., Zhang, Q., 2008. Anal. Chem. 80 (18), 7075–7083.
Weng, J., Zhang, Z., Sun, L., Wang, J.A., 2011. Biosens. Bioelectron. 26 (5), 1847–1852.
Xu, S.L., Liu, J.Y., Wang, T.S., Li, H.L., Miao, Y.Q., Liu, Y.Q., Wang, J., Wang, E.K., 2013. Talanta 104, 122–127.
Xu, Y., Xie, X., Duan, Y., Wang, L., Cheng, Z., Cheng, J., 2016. Biosens. Bioelectron. 77, 824–836.
Yoon, H.J., Kim, T.H., Zhang, Z., Azizi, E., Pham, T.M., Paoletti, C., Lin, J., Ramnath, N., Wicha, M.S., Hayes, D.F., Simeone, D.M., Nagrath, S., 2013. Nat. Nanotechnol. 8 (10), 735–741.
Yoon, H.J., Shanker, A., Wang, Y., Kozminsky, M., Jin, Q., Palanisamy, N., Burness, M.L., Azizi, E., Simeone, D.M., Wicha, M.S., Kim, J., Nagrath, S., 2016. Adv. Mater. 28 (24), 4891–4897.
Zhang, D.D., Zhang, Y.M., Zheng, L., Zhan, Y.Z., He, L.C., 2013. Biosens. Bioelectron. 42, 112–118.